Mass measurements in the vicinity of the doubly magic waiting point ^{56}Ni

A. Kankainen,* V.-V. Elomaa,† T. Eronen, D. Gorelov, J. Hakala, A. Jokinen, T. Kessler, V. S. Kolhinen, I. D. Moore, S. Rahaman,‡ M. Reponen, J. Rissanen, A. Saastamoinen, C. Weber,§ and J. Äystö

Department of Physics, University of Jyväskylä, P.O. Box 35, FI-40014 University of Jyväskylä, Finland

(Received 6 July 2010; published 13 September 2010)

Masses of ^{56,57}Fe, ^{53}Co^{m}, ^{53,56}Co, ^{55,56,57}Ni, ^{57,58}Cu, and ^{59,60}Zn have been determined with the JYFLTRAP Penning trap mass spectrometer at the Ion-Guide Isotope Separator On-Line facility with a precision of $\delta m/m \leqslant 3 \times 10^{-8}$. The Q_{EC} values for ^{53}Co, ^{55}Ni, ^{56}Ni, ^{57}Cu, ^{58}Cu, and ^{59}Zn have been measured directly with a typical precision of better than 0.7 keV and Coulomb displacement energies have been determined. The Q values for proton captures on ^{55}Co, ^{56}Ni, ^{58}Cu, and ^{59}Cu have been measured directly. The precision of the proton-capture Q value for ^{56}Ni$(p,\gamma)^{57}$Cu, $Q_{(p,\gamma)} = 689.69(51)$ keV, crucial for astrophysical rp-process calculations, has been improved by a factor of 37. The excitation energy of the proton-emitting spin-gap isomer ^{53}Co^{m} has been measured precisely, $E_x = 3\,174.3(10)$ keV, and a Coulomb energy difference of 133.9(10) keV for the $19/2^-$ state has been obtained. Except for ^{53}Co, the mass values have been adjusted within a network of 17 frequency ratio measurements between 13 nuclides, which allowed also a determination of the reference masses ^{55}Co, ^{58}Ni, and ^{59}Cu.

DOI: 10.1103/PhysRevC.82.034311 PACS number(s): 21.10.Dr, 21.10.Sf, 27.40.+z, 27.50.+e

I. INTRODUCTION

^{56}Ni is a waiting-point nucleus in the astrophysical rapid-proton-capture process (rp process), a sequence of proton captures and β^+ decays occurring at high temperatures and high hydrogen densities, such as in x-ray bursts (see, e.g., Ref. [1]). In the rp process, nuclides capture protons until they are inhibited by a low or negative Q value. At such waiting points, the process must proceed via much slower β decay. At ^{56}Ni, the proton-capture Q value to ^{57}Cu is quite low and critical for the synthesis of elements heavier than nickel. Namely, the β-decay half-life of ^{56}Ni is 6.075(10) days [2], exceeding all normal time scales of x-ray bursts and other places where the rp process could occur. Previously, ^{56}Ni was considered as the end point of the rp process [3], but later it was shown to proceed until the SnSbTe region [4,5]. Detailed modeling of the rp process is needed for thorough understanding of energy release, light curves, dynamics of hydrogen burning, and abundance patterns, for example, in x-ray bursts. For an accurate modeling of this process, the proton-capture Q value for the reaction ^{56}Ni$(p,\gamma)^{57}$Cu has to be known precisely.

^{56}Ni is doubly magic and therefore the precise knowledge of its mass and the masses of the neighboring nuclei is important for nuclear structure studies around $Z = N = 28$. Nuclei close to or at the $N = Z$ line offer an interesting possibility to study the exchange symmetry between neutrons and protons. The Q_{EC} values between the isospin $T = 1/2$ mirror nuclei provide direct information on the Coulomb displacement energies, in other words, the binding energy differences between two adjacent members of an isobaric multiplet. By plotting the Coulomb energy differences, i.e., the differences in the level excitation energies of mirror nuclei, as a function of the spin, interesting information on changes in nuclear structure can be obtained. One of the mirror nuclei close to ^{56}Ni is ^{53}Co, which has a renowned spin-gap isomer ^{53}Co^{m} $(19/2^-)$ from which direct proton decay was observed for the first time [6,7]. A precise and direct measurement of this excitation energy is needed for an accurate Coulomb energy difference value of the ^{53}Co $19/2^-$ state.

Recently, the Q_{EC} values of lighter $T = 1/2$ nuclei have been used to determine high-precision corrected ft values. From the corrected ft values, a mixing ratio of Fermi and Gamow-Teller transitions is obtained [8]. This mixing ratio is useful for testing the standard model values for the β-decay correlation coefficients [8], such as the β-neutrino angular correlation coefficient. If the β asymmetry parameter A_β, neutrino asymmetry parameter B_ν, or β-neutrino angular correlation coefficient $a_{\beta\nu}$ has already been measured, the mixing ratio can be determined and the $|V_{ud}|$ value for the Cabibbo-Kobayashi-Maskawa matrix can be extracted from the corrected ft values [9]. This, in turn, provides an opportunity to test the conserved vector current hypothesis.

II. EXPERIMENTAL METHODS

The studied neutron-deficient nuclides were produced at the Ion-Guide Isotope Separator On-Line (IGISOL) facility [10]. In the first run, proton or ^{3}He^{2+} beams from the K-130 cyclotron impinging on enriched ^{54}Fe (2 mg/cm^2) or ^{58}Ni (1.8 mg/cm^2) targets produced the ions of interest employing the light-ion ion guide [11]. The corresponding proton beam intensity was about 10 μA and the ^{3}He^{2+} beam 0.5 $p\mu$A. A 50 MeV proton beam was used to test the production of ^{54}Ni

*anu.k.kankainen@jyu.fi

†Present address: Turku PET Centre, Accelerator Laboratory, Åbo Akademi University, FI-20500 Turku, Finland.

‡Present address: Physics Division, P-23, Mail Stop H803, Los Alamos National Laboratory, Los Alamos, NM 87545, USA.

§Present address: Department of Physics, Ludwig-Maximilians-Universität München, D-85748 Garching, Germany.

TABLE I. Properties of the nuclides studied in this work taken from Ref. [12]. Given are the half-lives ($T_{1/2}$), spins (I), parities (π), and excitation energies of the isomers (E_x).

Nuclide	$T_{1/2}$	I^π	E_x (keV)
^{56}Fe	Stable	0^+	
^{57}Fe	Stable	$1/2^-$	
^{53}Co	244.6(76) ms[a]	$7/2^-$#[b]	
^{53}Co^m	247(12) ms	$(19/2^-)$	3197(29)
^{55}Co	17.53(3) h	$7/2^-$	
^{56}Co	77.23(3) d	4^+	
^{55}Ni	203.3(37) ms[a]	$7/2^-$	
^{56}Ni	6.075 (10) d	0^+	
^{57}Ni	35.60(6) h	$3/2^-$	
^{58}Ni	Stable	0^+	
^{57}Cu	196.44(68) ms[a]	$3/2^-$	
^{58}Cu	3.204(7) s	1^+	
^{59}Cu	81.5(5) s	$3/2^-$	
^{59}Zn	181.9(18) ms[a]	$3/2^-$	
^{60}Zn	2.38(5) min	0^+	

[a]The half-life taken from Ref. [8].
[b]'#' indicates a value that is estimated from systematic trends from neighboring nuclides with the same Z and N parities.

and ^{56}Cu. However, these exotic nuclides were not observed in this run. The properties of the studied nuclides are summarized in Table I and the production methods in Table II.

In the second run, the ions of interest were searched for via heavy-ion fusion-evaporation reactions with a $^{20}Ne^{4+}$ beam impinging on a calcium target (4 mg/cm^2) at 75 and 105 MeV. Previously, the heavy-ion ion guide (HIGISOL) [14] has been successfully used for producing heavier nuclides for JYFLTRAP mass measurements [5,15,16]. This was the first experiment performed in a lighter-mass region. At HIGISOL, the target wheel is located along the cyclotron beamline before the gas cell and the primary heavy-ion beam is stopped in a graphite beam dump before entering the cell to avoid plasma effects. This sets two requirements for the recoiling reaction products: they have to scatter at large enough angles and they have to have sufficient energy to pass through the entrance window around the gas cell. The $^{20}Ne + ^{40}Ca$ reaction gave enough angular spread for the recoils but not enough energy for them to pass sufficiently through a 2-mg/cm^2-thick Havar entrance window to the HIGISOL gas cell. Therefore, only ^{57}Ni and ^{56}Co were measured against ^{58}Ni in this latter run.

As the masses determined in this work are derived from the frequency ratios measured against well-known reference masses, a small network of measured frequency ratios (or energy differences) between different nuclides forming a series of linked linear equations yields more accurate results for the mass values. In order to obtain more links between the nuclides in the network, an additional experiment was conducted at IGISOL where stable, well-known reference ions $^{56}Fe^+$, $^{57}Fe^+$, and $^{58}Ni^+$ were produced with an offline electric discharge ion source [17] and the frequency ratios between these nuclides were measured with JYFLTRAP.

After extraction from the gas cell, the ions were accelerated to 30 keV and mass-separated by a 55° dipole magnet. The ions with the same mass number A were sent to a radio-frequency

TABLE II. The measured frequency ratios ($r = \nu_{ref}/\nu_c$) for the nuclides. The references used, the production method, the number of measurements (N_{meas}), and the total number of ions in the resonances (N_{ions}) are also given in the table. Note that the frequency ratios of ^{56}Co and ^{57}Ni relative to ^{58}Ni were measured in the HIGISOL run, and the last three frequency ratios in an offline run employing an electric discharge ion source. Uncertainties in the frequency ratios are given without (δr) and with an additional relative residual uncertainty of 7.9×10^{-9} [13] (δr_{all}).

Nuclide	Ref.	Prod. Method	N_{meas}	N_{ions}	$r(\delta r)(\delta r_{all})$
^{53}Co	^{53}Fe	40 MeV p on ^{54}Fe	9	30 731	1.000 168 055 7(46)(92)
^{53}Co^m	^{53}Fe	40 MeV p on ^{54}Fe	6	5 152	1.000 232 415(23)(24)
^{53}Co^m	^{53}Co	40 MeV p on ^{54}Fe	4	3 122	1.000 064 357(27)(28)
^{55}Ni	^{55}Co	25 MeV $^3He^{2+}$ on ^{54}Fe	6	5 690	1.000 169 879 6(81)(113)
^{56}Ni	^{55}Co	40 MeV p on ^{58}Ni	4	12 644	1.018 203 600 5(36)(88)
^{56}Ni	^{56}Co	25 MeV $^3He^{2+}$ on ^{54}Fe	4	9 861	1.000 040 930 2(39)(88)
^{56}Ni	^{56}Fe	50 MeV p on ^{58}Ni	4	24 970	1.000 128 579 3(48)(92)
^{57}Cu	^{56}Ni	40 MeV p on ^{58}Ni	6	9 460	1.018 002 434 0(57)(99)
^{57}Cu	^{57}Ni	40/50 MeV p on ^{58}Ni	11	10 895	1.000 165 446 9(56)(97)
^{57}Cu	^{57}Fe	40 MeV p on ^{58}Ni	5	8 020	1.000 242 695(13)(15)
^{58}Cu	^{58}Ni	40 MeV p on ^{58}Ni	7	20 384	1.000 158 637 1(33)(86)
^{59}Zn	^{58}Cu	25 MeV $^3He^{2+}$ on ^{58}Ni	2	1 399	1.017 340 531(21)(22)
^{59}Zn	^{59}Cu	25 MeV $^3He^{2+}$ on ^{58}Ni	5	6 741	1.000 166 532 0(93)(122)
^{60}Zn	^{58}Ni	25 MeV $^3He^{2+}$ on ^{58}Ni	6	15 744	1.034 633 758 6(49)(95)
^{60}Zn	^{59}Cu	25 MeV $^3He^{2+}$ on ^{58}Ni	5	9 786	1.017 006 490 0(48)(94)
^{56}Co	^{58}Ni	105 MeV $^{20}Ne^{4+}$ on ^{nat}Ca	6	21 159	0.965 556 038 7(54)(94)
^{57}Ni	^{58}Ni	75 MeV $^{20}Ne^{4+}$ on ^{nat}Ca	5	5 726	0.982 816 024 9(96)(124)
^{56}Fe	^{58}Ni	Discharge ion source	20	119 485	0.965 471 417 0(26)(81)
^{57}Fe	^{56}Fe	Discharge ion source	14	55 197	1.017 886 256 4(21)(83)
^{57}Fe	^{58}Ni	Discharge ion source	21	98 650	0.982 740 085 8(17)(80)

quadrupole cooler and buncher [18], which delivered the ions as short, cooled bunches to the JYFLTRAP Penning trap mass spectrometer [19]. JYFLTRAP consists of two cylindrical Penning traps inside a $B = 7$ T superconducting solenoid. The first trap, the *purification trap*, is used for selecting the isobar (in some cases even the isomer) of interest via mass-selective buffer gas cooling [20]. After the first trap, the ions were sent to the second trap, the *precision trap*, where the masses of the ions m with a charge q were measured precisely by determining the cyclotron frequency $\nu_c = qB/(2\pi m)$ via a time-of-flight (TOF) ion cyclotron resonance method [21,22]. The cyclotron frequency was obtained by measuring the sideband frequency $\nu_+ + \nu_-$, where ν_+ and ν_- are the reduced cyclotron and magnetron frequencies, respectively. The sideband frequency corresponds to the cyclotron frequency at very high precision [23]. Possible frequency shifts of the JYFLTRAP Penning trap have been carefully studied in Ref. [13] and have been accounted for in the analysis procedure.

Conventionally, the resonance curve is obtained with a quadrupolar rf field with a typical duration of 200–800 ms. Recently, a Ramsey method of time-separated oscillatory fields has been applied to short-lived ions in Penning traps [24,25]. The Ramsey method decreases the linewidth of the resonance and makes the sidebands much stronger, resulting in a considerably smaller statistical uncertainty in the cyclotron frequency. The Ramsey excitation scheme and a new method of Ramsey cleaning have been successfully applied at JYFLTRAP [26]. In the new cleaning mode, the ions from the purification trap are excited by a time-separated oscillatory electric dipole field in the precision trap. The undesired ions are driven into a larger orbit while the ions of interest remain unaffected if an appropriate dipole excitation pattern is chosen. After that, the ions of interest are sent back to the purification trap whereas the unwanted ions cannot pass through the 2-mm diaphragm between the traps. In the purification trap, the ions of interest are recentered and returned once more to the precision trap for the final mass measurement. A so-called back-and-forth scheme is similar to the Ramsey cleaning scheme except that no dipole excitation in the precision trap is applied before sending the ions back to the purification trap, resulting in much smaller bunch size.

In this work, normal (conventional) TOF resonances were measured for all ions in order to be sure about the center frequency in the Ramsey excitation scheme. The duration of the Ramsey fringes was 25 ms. The waiting time between the two fringes was 350 ms for the long-lived nuclide ^{56}Ni and its references and 150 ms for the other, shorter-lived nuclides and their references. Only ^{60}Zn and its references were measured with the conventional TOF method with a quadrupolar excitation period of 800 ms. Ramsey cleaning with a 25 ms–30 ms–25 ms dipole excitation scheme was applied for ^{55}Co and ^{55}Ni. For ^{56}Ni, ^{57,58}Cu, and ^{59}Zn and their references (except ^{55}Co) a back-and-forth scheme was used. In the HIGISOL run, a 25 ms–150 ms–25 ms excitation pattern with the back-and-forth purification was used for ^{56}Co, ^{57}Ni, and ^{58}Ni. In the run employing the electric discharge ion source, a 25 ms–350 ms–25 ms excitation pattern with the back-and-forth purification was used for ^{56,57}Fe and ^{58}Ni.

III. DATA ANALYSIS

A. Analysis of the measured frequency ratios

The cyclotron resonance frequencies were fitted with the theoretical line shape [22,24,25] (see Fig. 1). The measured frequencies were corrected for the count-rate effect [27] whenever it was possible. For the lower-statistics files, where the count-rate-class analysis was not possible, the statistical error was multiplied by a factor obtained from a comparison of the errors in the frequencies of all higher-statistics files with and without the count-rate-class analysis. The magnetic field B at the time of measurement was interpolated from the well-known reference measurements before and after the measurement. The frequency ratio r of the well-known reference ion to the ion of interest was determined [see Eq. (1)]. This ratio gives the mass ratio of the ion of interest to the reference ion [see Eq. (2)],

$$r = \frac{\nu_{\mathrm{ref}}}{\nu}, \tag{1}$$

$$r = \frac{m - m_e}{m_{\mathrm{ref}} - m_e}. \tag{2}$$

In order to take into account fluctuations in the magnetic field, a correction of $\delta_B(\nu_{\mathrm{ref}})/\nu_{\mathrm{ref}} = [5.7(8) \times 10^{-11}\ \mathrm{min}^{-1}]\Delta t$, where Δt is the time between the two reference measurements, was quadratically added to the statistical uncertainty of each frequency ratio. The weighted mean of the measured frequency ratios was calculated and used as the final value. The inner and outer errors [28] of the data sets were compared and the larger value of these two was taken as the error of the mean. Finally, the uncertainty due to mass-dependent shift $\delta_{m,\mathrm{lim}}(r)/r = (7.5 \pm 0.4 \times 10^{-10}/u) \times \Delta m$ [13] and an additional residual relative uncertainty $\delta_{\mathrm{res,lim}}(r)/r = 7.9 \times 10^{-9}$ [13] were quadratically added to the error.

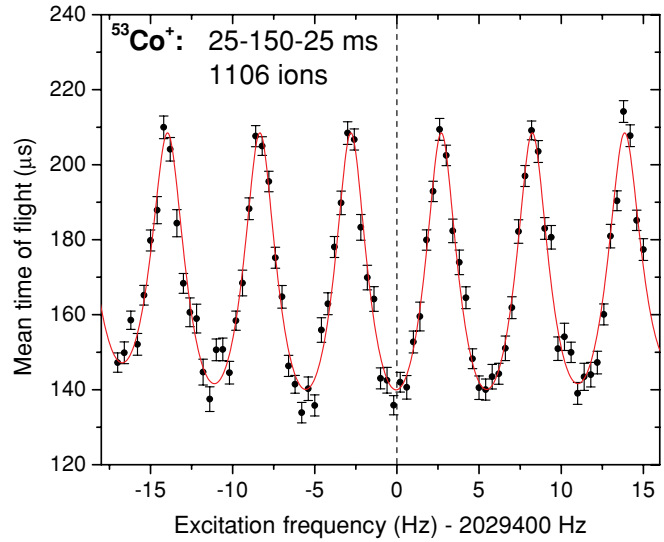

FIG. 1. (Color online) Cyclotron resonance curve for ^{53}Co$^+$. Ramsey excitation with a 25 ms–150 ms–25 ms (on-off-on) pattern was used. Only bunches having one single ion are shown.

B. Data evaluation

In order to evaluate the masses of the measured nuclides, a least-squares adjustment was done in a similar manner as in Refs. [29–31]. Here, we follow the notations used in those references. The input data q_i for the least-squares method consist of the measured 17 frequency ratios between 13 nuclides (see Table II) and the current mass values for the 13 nuclides from the Atomic Mass Evaluation 2003 (AME03) [29]. Thus, we have 30 input data to 13 nuclides involved in the frequency ratio measurements, forming an overdetermined system.

The input data of the 13 AME03 values are simply $q_i = m_i \pm \delta m_i$. For the frequency ratios, a similar procedure as in Ref. [31] was applied. Equation (2) can be expressed as a linear equation in m:

$$m - rm_{\mathrm{ref}} = m_e(1 - r). \tag{3}$$

In order to have the left side independent of the ratio r, a constant factor $C = A/A_{\mathrm{ref}}$, where A and A_{ref} are the mass numbers of the reference ion and the ion of interest, is introduced. Then, a term $-Cm_{\mathrm{ref}}$ is added on both sides of Eq. (3):

$$m - Cm_{\mathrm{ref}} = (r - C)m_{\mathrm{ref}} + m_e(1 - r). \tag{4}$$

Including the uncertainties δr, δm_{ref}, and δm_e, Eq. (4) yields

$$\begin{aligned} m - Cm_{\mathrm{ref}} = {} & (r - C)m_{\mathrm{ref}} + m_e(1 - r) \\ & + [(r - C)\delta m_{\mathrm{ref}} + m_{\mathrm{ref}}\delta r]. \end{aligned} \tag{5}$$

In Eq. (5), the terms $\delta m_e(1 - r)$ and $m_e\delta r$ have been neglected since they are small compared to $m_{\mathrm{ref}}\delta r$. Since the left side of Eq. (5) is a continuous and differentiable function of m, a least-squares fit to this linear, overdetermined system can be applied following Ref. [30]. The measured data q_i are obtained from Eq. (6) with the uncertainties dq_i given in Eq. (7):

$$q_i = (r - C)m_{\mathrm{ref}} + m_e(1 - r), \tag{6}$$

$$dq_i = (r - C)\delta m_{\mathrm{ref}} + m_{\mathrm{ref}}\delta r. \tag{7}$$

Let the vector $|m\rangle$ represent the masses of 13 nuclides involved in the frequency ratio measurements and the vector $|q\rangle$ corresponds to the input data [17 rows obtained from Eq. (6) and 13 rows representing the AME03 mass values of the nuclides]. Then, a 30×13 matrix K representing the coefficients $K|m\rangle = |q\rangle$ and a 30×30 diagonal weight matrix W with the elements $w_i^i = 1/dq_i^2$ can be formed. The solution of the least-squares method yields a vector of adjusted masses $|\overline{m}\rangle = A^{-1}{}^t K W|q\rangle = R|q\rangle$, where A^{-1} is the inverse of the normal matrix $A = {}^t KWK$, which is a positive-definite and invertible square matrix of the order of 13. The errors for the adjusted masses $\overline{m_i}$ are obtained as a square root of the diagonal elements of the matrix A^{-1}.

The adjusted data $|\overline{q}\rangle$ can be calculated as $|\overline{q}\rangle = KR|q\rangle$. Now, if the uncertainties dq_i are very small for this overdetermined system [the number of input data $N_d = 30$ is greater than the number of variables (masses) $N_v = 13$], the normalized deviation between the adjusted data $\overline{q_i}$ and input data q_i should have a Gaussian distribution with $\sigma = 1$. For $N_d - N_v = 30 - 13 = 17$ degrees of freedom, this gives a χ^2 equal to

$$\chi^2 = \sum_{i=1}^{N_d} \left(\frac{\overline{q_i} - q_i}{dq_i} \right)^2. \tag{8}$$

The consistency can also be expressed as normalized χ:

$$\chi_n = \sqrt{\chi^2/(N_d - N_v)}, \tag{9}$$

for which the expected value is $1 \pm 1/\sqrt{2(N_d - N_v)}$.

The influence of each datum i on a mass m_v can be seen from the (i, v) element of a flow-of-information matrix $F = {}^t R \otimes K$ (30×13 matrix) [30]. Each column of F represents all the contributions from all input data to a given mass m_v. The sum of these contributions is 1. The sum of influences along each row shows the significance of that datum.

IV. RESULTS AND DISCUSSION

A. Frequency ratios

Altogether 20 frequency ratios were measured in this work (see Table II and Fig. 2). The number of measured frequency ratios is high because the reference nuclides in this mass region are known with quite a modest precision of about 0.6–2 keV or $\delta m/m \approx (1.1\text{–}4.1) \times 10^{-8}$. Therefore, a small network of measurements provides more accurate mass values for the measured nuclides. In addition, some Q_{EC} and S_p values were measured directly to obtain a better precision.

B. Mass excess values

The nuclides other than ^{53}Co and ^{53}Co^m formed a network of 13 nuclides and 17 measured frequency ratios. For these nuclides, a least-squares method described in Sec. III B was applied and adjusted mass values were obtained. The normalized $\chi = 1.08$ was well within the expected value 1.00 ± 0.17, and therefore no additional error was added to the frequency ratios. The biggest contribution to the χ^2 value (27%) comes from the ^{58}Cu AME03 mass value which is

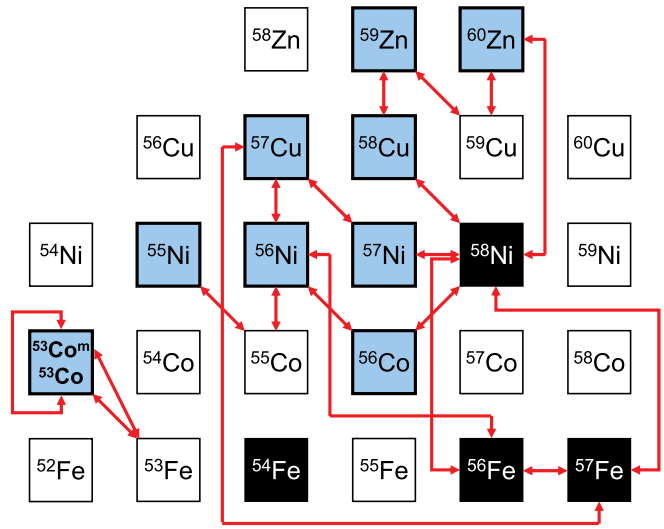

FIG. 2. (Color online) The highlighted nuclides were measured in this work. The red arrows show the measured frequency ratio pairs.

3.6(17) keV higher than the adjusted value obtained with the JYFLTRAP results. In addition to ^{58}Cu, the AME03 values of ^{55}Co (13%), ^{60}Zn (10%), ^{59}Zn (8%), and ^{58}Ni (7%) also have a substantial contribution to the χ^2 value. This is also seen in the adjusted values, which deviate from the AME03 values of these nuclides.

In the following, the mass excess results for the radioactive nuclides are compared to earlier experiments (see Figs. 3, 5, 6, and 7) and discussed nuclide by nuclide. The results for the nuclides mainly used as references are also summarized (see Figs. 8, 9, and 10). The directly measured values were used for ^{53}Co and ^{53}Co^m. For the rest, the adjusted mass values (see Table III) were applied. The results of ^{53}Co and ^{53}Co^m include also a new value for the excitation energy of the high-spin isomer.

1. ^{53}Co and the spin-gap isomer in ^{53}Co

The ground state mass of ^{53}Co in AME03 is based on the measured Q value of the ^{58}Ni(p,^{6}He)^{53}Co reaction [32], which is in agreement with the new JYFLTRAP value. Proton decay of the spin-gap isomer ^{53}Co^m was observed in Refs. [6,7]. The observed proton peak energies $E_{\rm lab} = 1\,570(30)$ keV [6] and $E_{\rm c.m.} = 1\,590(30)$ keV [7] and the tabulated mass of ^{52}Fe [29] result in an excitation energy of 3 197(29) keV and a mass excess value of $-39\,447(22)$ keV for ^{53}Co^m. The new JYFLTRAP mass excess value for the isomer agrees with the one from Ref. [7] but disagrees with the value of Ref. [6] and the adopted AME03 value [29] (see Fig. 3).

The excitation energy of the isomer was measured directly in the ^{53}Co^m-^{53}Co pair yielding an energy of 3 174.5(14) keV. It was also determined indirectly from the energy difference of the ^{53}Co^m-^{53}Fe and ^{53}Co-^{53}Fe pairs, resulting in an excitation energy of 3 174.1(13) keV. The weighted average of these results gives an excitation energy of 3 174.3(10) keV. With the ^{52}Fe mass excess from Ref. [29], this would correspond to a proton peak energy of $E_{\rm lab} = 1\,530(7)$ keV. A new decay scheme for ^{53}Co based on this work is presented in Fig. 4. Coulomb energy differences (CEDs) show the differences in the excitation energies between excited isobaric analog states (IASs) with increasing spin. The isobaric analog state of the $19/2^-$ isomer at $E_x = 3\,174.3(10)$ keV in ^{53}Co lies at 3 040.4(3) keV in ^{53}Fe. This yields a CED of 133.9(10) keV, which improves the precision considerably compared to the AME03 value of 157(29) keV. The new excitation energy for the isomer is quite close to the erroneous excitation energy of 3 179(30) keV adopted accidentally in Ref. [33] instead of the AME03 value of 3 197(29) keV [29]. Thus, the new result for the CED is (by chance) in agreement with the result of Ref. [33], where a smooth rise of CED was observed from the $7/2^-$ state to the $19/2^-$ isomeric state. This smooth rise reflects the gradual alignment of the $\nu(f_{7/2})^{-2}$ pair from $J = 0$ to $J = 6$ in ^{53}Co [for the $\pi(f_{7/2})^{-2}$ pair in ^{53}Fe] [33,34].

2. ^{55}Ni

The mass of ^{55}Ni has been previously measured via ^{58}Ni(^{3}He,^{6} He)^{55}Ni reactions at the Michigan State University in the 1970s [32,35,36] and via a β-end-point measurement conducted at IGISOL [37]. The AME03 mass excess value is based on the Q value of Ref. [32] corrected by a new Q value for the calibration reaction ^{27}Al(^{3}He,^{6}He)^{24}Al used in Ref. [36]. The new JYFLTRAP value agrees with all the other values except with Ref. [35] for which the Q values used in the energy calibration are not given (see Fig. 5).

3. ^{56}Ni

The current mass excess value of ^{56}Ni is based on the Q values of the reactions ^{58}Ni(p,t)^{56}Ni [38] and ^{54}Fe(^{3}He,n)^{56}Ni [39]. Recently, prompt proton decay ($E_p = 2540(30)$ keV) was observed from a level at 9 735(2) keV in a rotational band of ^{56}Ni [40]. The JYFLTRAP value agrees with all previous experiments (see Fig. 5) but is 26 times more accurate than the adopted value.

4. ^{57}Cu

The mass of ^{57}Cu has been earlier determined via β-end-point energy [41], the Q values of ^{58}Ni(^{7}Li,^{8}He)^{57}Cu measured at the National Superconducting Cyclotron Laboratory [42] and at the Texas A & M cyclotron [43] and the Q value of ^{58}Ni(^{14}N,^{15}C)^{57}Cu [44]. The JYFLTRAP value is 31 times more accurate than the adopted AME03 value and in agreement with these measurements (see Fig. 6).

5. ^{58}Cu

The mass of ^{58}Cu was earlier based on the measurements of the threshold energy for the reaction ^{58}Ni(p, n)^{58}Cu [45–47]. The $Q_{\rm EC}$ value for ^{58}Cu has been measured at JYFLTRAP, $Q_{\rm EC} = 8\,555(9)$ keV [19] which yields a mass excess of $-51\,673(9)$ keV when using the AME03 value for ^{58}Ni. The new mass excess value of $-51\,665.69(52)$ keV disagrees with the (p, n) threshold energies and with the AME03 value but is in agreement with the previous JYFLTRAP result [19] and the result derived from prompt proton emission from ^{58}Cu [48].

The problems in the determination of the Q values from the threshold energies explain the discrepancy between the results. Freeman [49] has suggested that if threshold energies are used to derive Q values for mass determination, the errors should be increased by some, albeit arbitrary, factor ($\sqrt{2}$ or 2). In addition, Refs. [47] and [50] only recalculate the values measured in Refs. [45,46]. Thus, Ref. [47] should not be averaged with Ref. [46]. A revised value is given in Ref. [49]. However, none of these values agree with JYFLTRAP (see Fig. 6). A similar deviation of $-5.3(39)$ keV is observed when the JYFLTRAP value for the ^{54}Co mass [51] is compared with the threshold energy for the reaction ^{54}Fe(p, n)^{54}Co [49].

6. ^{59}Zn

The JYFLTRAP mass excess value for ^{59}Zn agrees with the mass derived from the $Q_{\rm EC}$ value of Ref. [52] and almost agrees with the value derived from the ^{58}Ni(p,π^-)^{59}Zn Q value [53].

TABLE III. Mass excess values (ME) and a comparison to literature values (ME_{AME}) [29]. The mass excess values are the adjusted values except for ^{53}Co and ^{53}Co^{m}, which were not included in the network.

Nuclide	ME (keV)	ME_{AME} (keV)	$ME-ME_{AME}$ (keV)	Input	Influence (%)
^{56}Fe	−60 605.38(37)	−60 605.4(7)	−0.03(78)	^{56}Fe-^{58}Ni	28.4
				^{57}Fe-^{56}Fe	24.9
				^{56}Ni-^{56}Fe	18.1
				^{56}Fe, AME03	28.6
^{57}Fe	−60 179.78(38)	−60 180.1(7)	0.35(78)	^{57}Fe-^{56}Fe	28.1
				^{57}Fe-^{58}Ni	32.8
				^{57}Cu-^{57}Fe	8.4
				^{57}Fe, AME03	30.8
^{53}Co[a]	−42 657.3(15)	−42 645(18)	−13(18)	^{53}Co-^{53}Fe	65.6
				^{53}Co-^{53}Co^{m}-^{53}Fe	34.4
^{53}Co^{m}[a]	−39 482.9(16)	−39 447(22)	−36(22)	^{53}Co^{m}-^{53}Fe	53.9
				^{53}Co^{m}-^{53}Co-^{53}Fe	46.1
^{55}Co	−54 028.72(48)	−54 027.6(7)	−1.16(87)	^{55}Ni-^{55}Co	0.2
				^{56}Ni-^{55}Co	56.1
				^{55}Co, AME03	43.7
^{56}Co	−56 038.81(47)	−56 039.4(21)	0.5(22)	^{56}Co-^{58}Ni	50.9
				^{56}Ni-^{56}Co	44.2
				^{56}Co, AME03	4.9
^{55}Ni	−45 334.69(75)	−45 336(11)	0.9(110)	^{55}Ni-^{55}Co	99.5
				^{55}Ni, AME03	0.5
^{56}Ni	−53 906.02(42)	−53 904(11)	−2.3(111)	^{56}Ni-^{55}Co	23.3
				^{56}Ni-^{56}Co	22.6
				^{56}Ni-^{56}Fe	35.8
				^{57}Cu-^{56}Ni	18.2
				^{56}Ni, AME03	0.1
^{57}Ni	−56 082.11(55)	−56 082.0(18)	−0.1(19)	^{57}Ni-^{58}Ni	46.5
				^{57}Cu-^{57}Ni	44.4
				^{57}Ni, AME03	9.1
^{58}Ni	−60 226.96(35)	−60 227.7(6)	0.74(70)	^{56}Fe-^{58}Ni	17.8
				^{57}Fe-^{58}Ni	18.3
				^{56}Co-^{58}Ni	8.8
				^{57}Ni-^{58}Ni	5.5
				^{58}Cu-^{58}Ni	6.5
				^{60}Zn-^{58}Ni	10.2
				^{58}Ni, AME03	33.0
^{57}Cu	−47 307.20(50)	−47 310(16)	2(16)	^{57}Cu-^{56}Ni	46.0
				^{57}Cu-^{57}Ni	27.3
				^{57}Cu-^{57}Fe	26.6
				^{57}Cu, AME03	0.1
^{58}Cu	−51 665.69(52)	−51 662.1(16)	−3.6(17)	^{58}Cu-^{58}Ni	78.2
				^{59}Zn-^{58}Cu	10.5
				^{58}Cu, AME03	11.3
^{59}Cu	−56 356.83(54)	−56 357.2(8)	0.40(95)	^{59}Zn-^{59}Cu	10.8
				^{60}Zn-^{59}Cu	42.4
				^{59}Cu, AME03	46.8
^{59}Zn	−47 213.93(74)	−47 260(40)	47(40)	^{59}Zn-^{58}Cu	29.8
				^{59}Zn-^{59}Cu	70.2
				^{59}Zn, AME03	0.04
^{60}Zn	−54 172.67(53)	−54 188(11)	15(11)	^{60}Zn-^{58}Ni	65.9
				^{60}Zn-^{59}Cu	33.8
				^{60}Zn, AME03	0.2

[a]The mass excess value has been determined with respect to the reference nucleus ^{53}Fe either directly or via ground or isomeric state for the isomeric or ground state, respectively. A weighted mean of these two values has been adopted for the mass excess value.

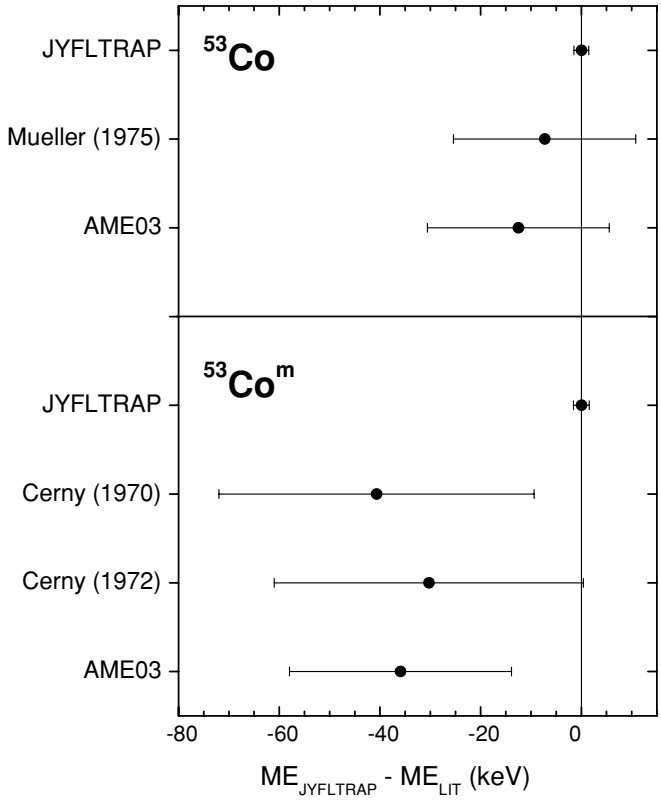

FIG. 3. Differences between the experimental mass excess values of the ground and isomeric states of ^{53}Co measured at JYFLTRAP with respect to the earlier experiments [6,7,32] and AME03 [29].

However, the AME03 value deviates from the JYFLTRAP value by slightly more than 1σ (see Fig. 7).

7. ^{60}Zn

The mass of ^{60}Zn is based on the Q values for the reaction ^{58}Ni(^{3}He,n)^{60}Zn [39,54] in the AME03 compilation. The new JYFLTRAP value agrees with the one from Ref. [39] but disagrees slightly with Ref. [54] and with the AME03 value. The Q_{EC} value for the β decay of ^{60}Zn [55] is in

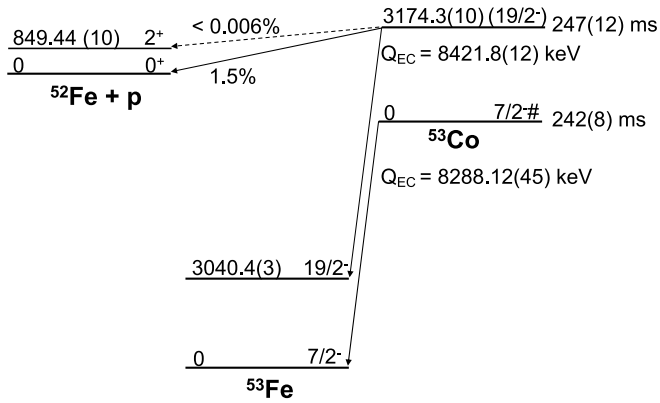

FIG. 4. Revised decay scheme of ^{53}Co. For the Q_{EC} values, see Sec. IV C.

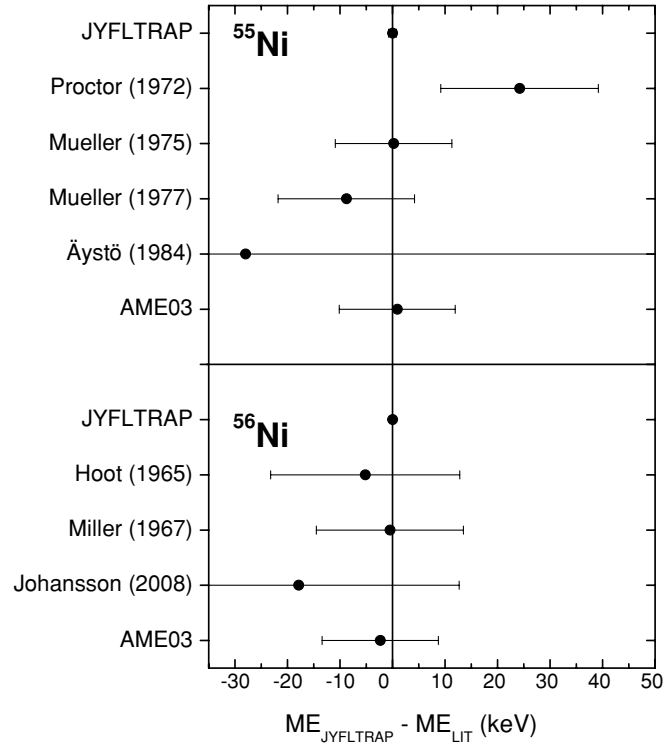

FIG. 5. Differences between the experimental mass excess values of the nickel isotopes measured at JYFLTRAP with respect to the earlier experiments [32,35–40] and AME03 [29].

agreement with the mass excess value measured in this work (see Fig. 7).

8. References ^{56,57}Fe, ^{55,56}Co, ^{57,58}Ni, and ^{59}Cu

Of the nuclides used as references in the frequency ratio measurements, ^{56}Ni and ^{58}Cu have already been discussed above. Here, we concentrate on other reference nuclides: ^{56,57}Fe, ^{55,56}Co, ^{57,58}Ni, and ^{59}Cu. Masses of these reference nuclides close to ^{56}Ni are known with a rather modest precision of 0.6–2.1 keV. However, with the network of mass measurements, the precisions of these mass excess values have been improved to 0.35–0.55 keV. The adjusted mass excess values for the used references agree well with the earlier results except for ^{55}Co, which deviates by $-1.16(87)$ keV from the AME03 value, and for ^{58}Ni, for which the deviation is 0.74(70) keV. The deviation at ^{55}Co is also seen in the mass excess values of ^{56}Ni with respect to different reference nuclides. The mass excess value obtained for ^{56}Ni with the ^{55}Co reference is significantly higher than the values obtained with ^{56}Co and ^{56}Fe references, suggesting that ^{55}Co might have a too high mass excess value in Ref. [29]. The former values of ^{55}Co are based on ^{54}Fe(p,γ)^{55}Co [56–58], ^{58}Ni(p,α)^{55}Co [59,60], and ^{54}Fe(^{3}He,d)^{55}Co [60]. Of these, only the first ^{54}Fe(p,γ)^{55}Co value [56] and the ^{54}Fe(^{3}He,d)^{55}Co value [60] agree with JYFLTRAP (see Fig. 8). The rest seem to overestimate the mass excess value.

For the reference ^{58}Ni, the earlier (n,γ) measurements [62,63] agree almost perfectly with the JYFLTRAP value

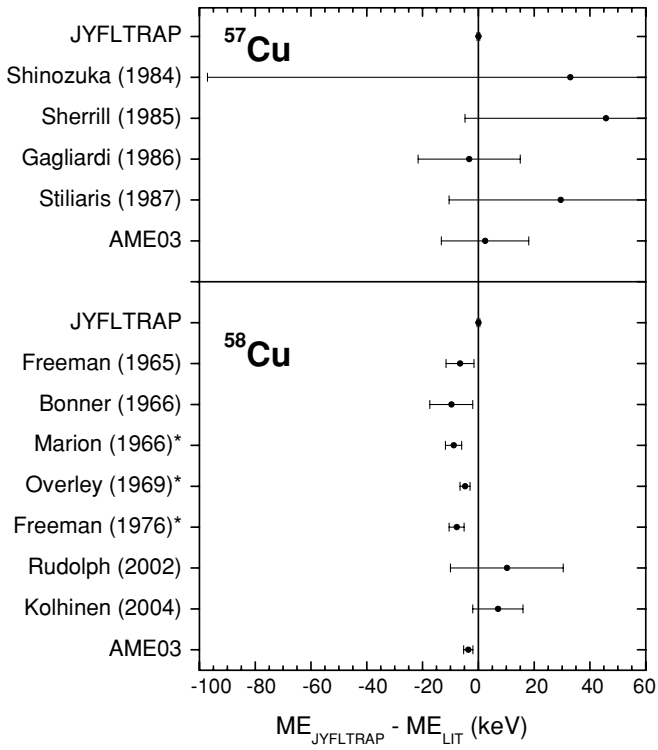

FIG. 6. Differences between the experimental mass excess values of the copper isotopes measured at JYFLTRAP with respect to the earlier experiments [19,41–50] and AME03 [29]. The values marked with $*$ are only recalculated values from previous (p, n) measurements of [45] and [46].

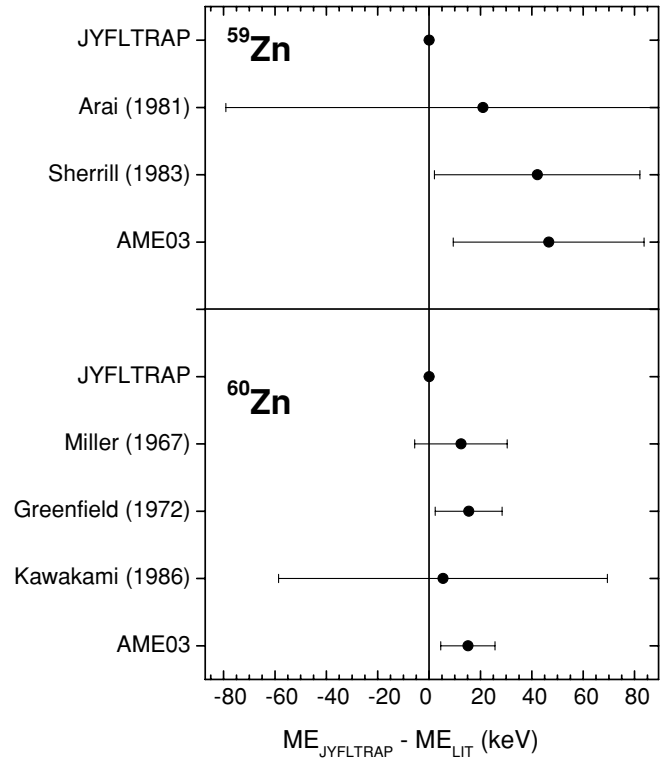

FIG. 7. Differences between the experimental mass excess values of the zinc isotopes measured at JYFLTRAP with respect to the earlier experiments [39,52–55] and AME03 [29].

whereas the newer mass excess values together with the AME03 value disagree with it by 1σ. Otherwise the iron and nickel reference nuclides agree surprisingly well with the earlier experiments (see Figs. 9 and 10), although many of these results have been measured precisely via (n,γ) reactions. This comparison shows that the uncertainties in the JYFLTRAP values are at a reasonable level. In addition, we could determine the neutron separation energies for ^{57}Fe and ^{58}Ni directly, resulting in $S_n = 7\,645.8(4)$ keV and $S_n = 12\,216.4(7)$ keV, in agreement with the AME03 values $S_n = 7\,646.10(3)$ keV and $S_n = 12\,217.0(18)$ keV for ^{57}Fe and ^{58}Ni, respectively. The adjustment procedure also improved the precision of the radioactive ^{59}Cu result from 0.8 to 0.54 keV. The new value agrees well with the AME03 value based on ^{58}Ni$(p,\gamma)^{59}$Cu reactions [75–77].

C. Q_{EC} values and mirror decays

The Q_{EC} values are directly obtained by measuring the frequency ratio r between the β-decay mother (mass m_m) and daughter (mass m_d) in a Penning trap:

$$Q_{\mathrm{EC}} = (m_m - m_d)c^2 = (r-1)(m_d - m_e)c^2. \qquad (10)$$

With this method, the Q_{EC} values can be determined to high precision even if the reference (daughter) nuclide has a moderate precision. The mass excesses for the daughter nuclides were taken from the adjusted mass values (Table III).

The Q_{EC} values are tabulated in Table IV. The mirror-decay Q_{EC} values of $T = 1/2$ nuclides ^{53}Co, ^{55}Ni, ^{57}Cu, and ^{59}Zn as well as the Q_{EC} values for the $T_Z = 0$ nuclides ^{56}Ni and ^{58}Cu in the $T = 1$ triplets at $A = 56$ and $A = 58$ were directly determined from the frequency ratio measurements against their β-decay daughters. In addition, the Q_{EC} value for the spin-gap isomer ^{53}Co^m was measured relative to the ^{53}Fe ground state. ^{53}Co^m decays dominantly to its isobaric analog state at 3040.4(3)keV in ^{53}Fe [78], for which a Q_{EC} value of 8421.8(12) keV is obtained. The Q_{EC} value for ^{60}Zn was determined from the adjusted mass value for ^{60}Zn and the AME03 value for ^{60}Cu [29].

Recently, corrected ft values, $\mathcal{F}t$, have been calculated for $T = 1/2$ mirror transitions up to ^{45}V [8,9]. The Q_{EC} values measured in this work offer a possibility to expand these studies from ^{53}Co up to ^{59}Zn. Table V summarizes the current averages of half-lives and branching ratios as well as electron-capture probabilities needed to calculate the ft value. Experimental Gamow-Teller matrix elements $|\langle\sigma\tau\rangle|$ have been calculated from the Gamow-Teller strength $B(\mathrm{GT})$:

$$B(\mathrm{GT}) = \frac{C}{ft} - B(\mathrm{F}),$$
$$\langle\sigma\tau\rangle^2 = \frac{B(\mathrm{GT})}{(g_A/g_V)^2}, \qquad (11)$$

where the constant $C = 2\overline{\mathcal{F}t}^{0^+\to 0^+} = 6\,143.5(17)$ s [80], $B(\mathrm{F})$ is the Fermi strength, which equals 1 for $T = 1/2$ mirror decays, and $g_A/g_V = -1.2\,695(29)$ [81] is the ratio of the

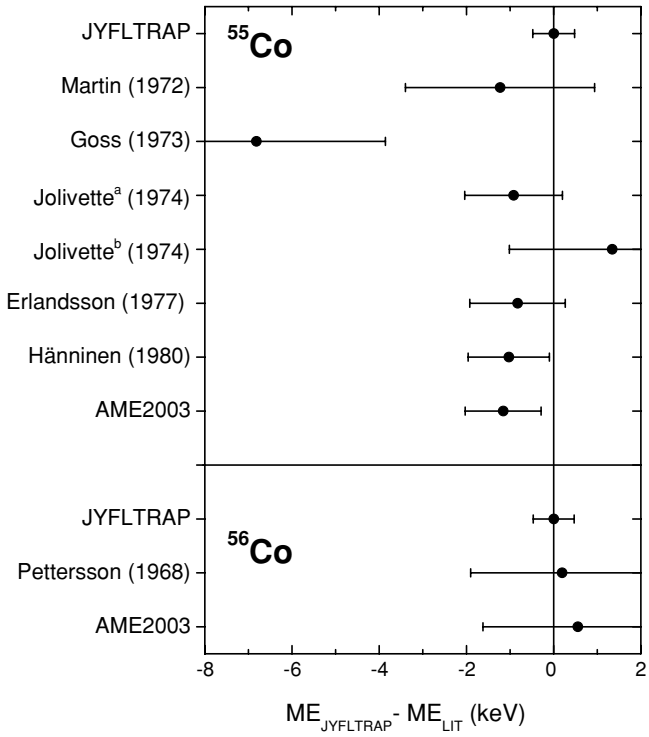

FIG. 8. Differences between the adjusted mass excess values of the cobalt isotopes used as references with respect to the earlier experiments [56–61] and AME03 [29]. ^{55}Co is discussed in the text and the ^{56}Co value of [61] is based on a β-end-point energy. Jolivette[a] refers to the ^{58}Ni(p,α)^{55}Co Q value [60] and Jolivette[b] to the ^{54}Fe(^{3}He,d)^{55}Co Q value [60].

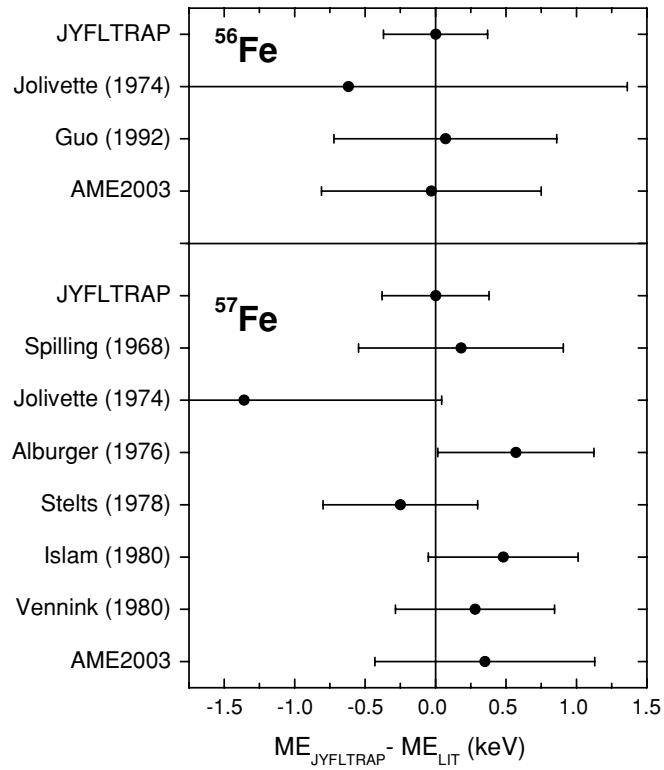

FIG. 9. Differences between the adjusted mass excess values of the iron isotopes used as references with respect to the earlier experiments and AME03 [29]. The earlier measurements are based on ^{59}Co(p,α)^{56}Fe [60] and ^{55}Mn(p,γ)^{56}Fe [64] for ^{56}Fe and on ^{56}Fe(n,γ)^{57}Fe [65–69] and ^{56}Fe(d,p)^{57}Fe [60].

axial vector to the vector coupling constant. Isospin symmetry breaking and radiative corrections have not been taken into account. Their effect would be less than 1% of the ft value, which is small compared to the overall uncertainty of the $|\langle\sigma\tau\rangle|$ values. As can be seen from Tables IV and V, the precisions of the ft and $|\langle\sigma\tau\rangle|$ values are still limited by the uncertainties in the half-lives and branching ratios.

The $Q_{\rm EC}$ value of ^{58}Cu is important for the calibration of the B(GT) values in ^{58}Ni(^{3}He,t)^{58}Cu charge-exchange reactions [82]. The measured $Q_{\rm EC}$ value, the half-life of 3.204(7) s [83] and an average branching ratio of 81.1(4)% for ^{58}Cu (from the values of 80.8(7)% [84], 81.2(5)% [85], and 82(3)% [86]) yields $\log ft = 4.8701(24)$ with the calculator in Ref. [79]. The obtained Gamow-Teller strength is B(GT) = 0.08 285(46) and the squared Gamow-Teller matrix element is $\langle\sigma\tau\rangle^2 = 0.05\,141(33)$. The values are little higher and more precise than previously [cf. B(GT) = 0.0 821(7) and $\langle\sigma\tau\rangle^2 = 0.0\,512(5)$ in Ref. [84]].

D. Coulomb displacement energies

If charge symmetry is assumed, the energy difference between the isobaric analog states in mirror nuclei is only caused by the Coulomb interaction and neutron-proton mass difference. If charge independence is assumed, the same is also true for isobaric triplets with $T = 1$.

The Coulomb displacement energy (CDE) is the total binding energy difference between the isobaric analog states in the neighboring isobars determined as CDE = $Q_{\rm EC} + \Delta_{n-{\rm H}}$, where $\Delta_{n-{\rm H}} = 782.34\,660(55)$keV is the neutron-hydrogen mass difference. The Coulomb displacement energies follow a straight line when plotted as a function of $(Z-0.5)/A^{1/3}$ (see, e.g., Ref. [87]) if a simple model for an evenly charged spherical nucleus is assumed. Deviations from the line reflect structural changes in the nuclei.

Coulomb displacement energies from JYFLTRAP for $T = 1/2$ mirror and $T = 1$ isobaric analog states of cobalt, nickel, copper, and zinc nuclides are plotted in Fig. 11. As can be seen from Fig. 11, the CDE values do not follow a straight line as a function of $(Z-0.5)/A^{1/3}$. This can be partly explained by different spins in the $T = 1/2$ states: the ground state spin changes from $7/2^-$, $T = 1/2$ to $3/2^-$, $T = 1/2$ at ^{57}Cu. As the protons in the p orbits have a larger radius than the protons in the f orbits, the Coulomb repulsion in ^{53}Co and ^{55}Ni filling the $1f_{7/2}$ proton shells is stronger than in ^{57}Cu and ^{59}Zn filling the $2p_{3/2}$ shells. Compared to the AME03 [29] values, the precision of the CDE values has now been improved considerably, and deviations have been found for ^{58}Cu, ^{59}Zn, and ^{60}Zn. The trend is a little smoother in the $T = 1$ states. There, it should be noted that the 0^+, $T = 1$ state is not always the ground state. The lowest $T = 1, 0^+$ state lies at 1 450.68(4) keV in ^{56}Co, at 7 903.7(10) keV in ^{56}Ni, and at 202.6(3) keV in ^{58}Cu. For ^{60}Zn, the 0^+, $T = 1$ level is not

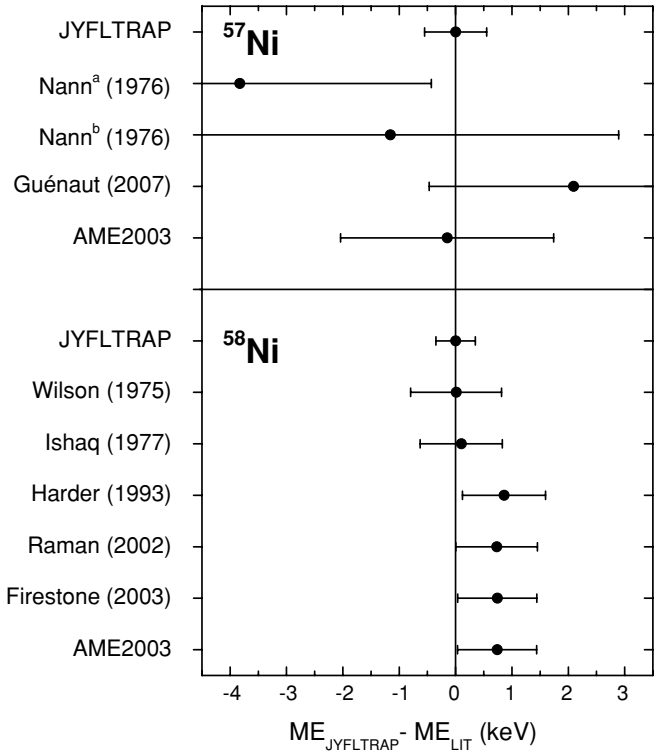

FIG. 10. Differences between the adjusted mass excess values of the nickel isotopes used as references with respect to the earlier experiments and AME03 [29]. The previous measurements are based on the Q values of ^{59}Ni$(p,t)^{57}$Ni (Nann[a]) [70] and ^{58}Ni$(^3$He,$\alpha)^{57}$Ni (Nann[b]) [70] and the frequency ratio for ^{57}Ni-^{85}Rb [71] for ^{57}Ni and the Q values for ^{58}Ni$(n,\gamma)^{59}$Ni [62,63,72–74] for ^{58}Ni.

known but the level at 4 913.1(9) keV is probably a $T = 1$ analog state of the ^{60}Cu 2^+ ground state [88], which has been adopted in Fig. 11. For the other nuclides in Fig. 11, the 0^+, $T = 1$ state is the ground state.

E. Proton-capture Q values for the rp process

Proton separation energies S_p (or proton-capture Q values) can be measured directly in a similar way as the Q_{EC} values

TABLE IV. The Q_{EC} values determined in this work. The values have been measured directly except for ^{60}Zn, for which the adjusted mass excess value has been used.

Nuclide	Q_{EC} (keV)	$Q_{EC,AME}$ [29] (keV)	JYFL-AME (keV)
^{53}Co	8 288.12(45)	8 300(18)	−12(18)
^{53}Co^m	11 462.2(12)[a]	11 498(22)	−36(22)
^{55}Ni	8 694.04(58)	8 692(11)	2(11)
^{56}Ni	2 132.76(46)	2 136(11)	−3(11)
^{57}Cu	8 775.07(51)	8 772(16)	3(16)
^{58}Cu	8 561.00(46)	8 565.6(14)	−4.6(15)
^{59}Zn	9 142.82(67)	9 097(40)	46(40)
^{60}Zn	4 171.4(18)[b]	4 156(11)	15(11)

[a] Q_{EC} value to the ^{53}Fe ground state.
[b] Based on the measured mass excess value and the mass of ^{60}Cu from Ref. [29].

TABLE V. The half-lives, electron capture probabilities (P_{EC}), branching ratios (BR), uncorrected log ft values, and experimental Gamow-Teller matrix elements $|\langle\sigma\tau\rangle|_{expt}$ for the mirror nuclei studied in this work. The average half-lives and branching ratios have been taken from Ref. [8]. The calculator from [79] was used for the P_{EC} and log ft values.

Parent nucleus	$t_{1/2}$ (ms)	P_{EC} (%)	BR (%)	log ft	$\lvert\langle\sigma\tau\rangle\rvert_{expt}$
^{53}Co	244.6(76)	0.099(2)	94.4(17)	3.625(17)	0.532(33)
^{55}Ni	203.3(37)	0.103(1)	100(10)	3.62(5)	0.54(10)
^{57}Cu	196.44(68)	0.103(1)	89.9(8)	3.670(5)	0.441(11)
^{59}Zn	181.9(18)	0.107(1)	94.03(77)	3.706(6)	0.360(14)

with a Penning trap. From the measured frequency ratio r between a nuclide (Z, A) with a mass m_m and the reference $(Z-1, A-1)$ with a mass m_d, a proton separation energy is obtained as

$$S_p = (-m_m + m_d + m_H)c^2 = [(1-r)(m_d - m_e) + m_H)]c^2, \quad (12)$$

where m_H is the mass of a hydrogen atom.

With this method, S_p values for ^{56}Ni, ^{57}Cu, ^{59}Zn, and ^{60}Zn were measured directly (see Table VI). The S_p values for ^{53}Co, ^{55}Ni, and ^{58}Cu were also improved with the new mass values of this work. The biggest differences from the AME03 values occur at ^{59}Zn and ^{60}Zn, which are now less proton-bound. The S_p value of ^{58}Cu differs slightly from the AME03 value.

In this work, we have improved the precisions of the Q values for the proton captures as well as the Q_{EC} values

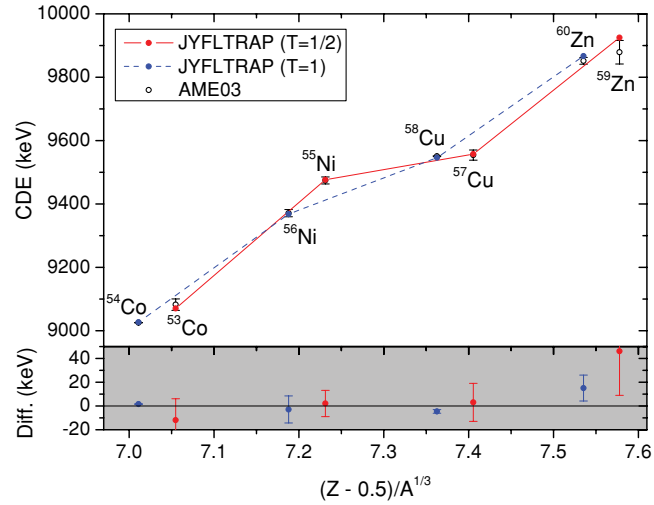

FIG. 11. (Color online) Coulomb displacement energies for the $T = 1/2$ doublets and $T = 1$ triplets in Co, Ni, Cu, and Zn isotopes from JYFLTRAP measurements and AME03 [29]. The JYFLTRAP Q_{EC} values are from this work except the value for ^{54}Mn which is from Ref. [51]. The lower panel shows the difference between the JYFLTRAP and AME03 values. For the $T = 1$ states, excitation energies have been taken into account. For the ^{60}Zn-^{60}Cu pair, a 0^+, $T = 1$ state is not known and therefore a 2^+, $T = 1$ state has been used.

TABLE VI. The S_p values determined in this work and comparison to the literature values [29]. The S_p values were measured directly with respect to the proton-decay daughters for ^{56}Ni, ^{57}Cu, ^{59}Zn, and ^{60}Zn. For the others, mass excess values determined in this work and literature values from Ref. [29] have been used.

Nuclide	S_p (keV)	$S_{p,\mathrm{AME}}$ [29] (keV)	JYFL-AME (keV)
^{53}Co[a]	1 615(7)	1 602(19)	13(20)
^{54}Ni[b]	3 842(50)	3 855(50)	−13(70)
^{55}Ni[c]	4 615.7(11)	4 617(11)	−1(11)
^{56}Ni	7 165.84(45)	7 165(11)	1(11)
^{56}Cu[b]	555(140)	554(140)	1(200)
^{57}Cu	689.69(51)	695(19)	−5(19)
^{58}Cu[a]	2 872.55(76)	2 869.1(24)	3.5(25)
^{58}Zn[b]	2 279(50)	2 277(50)	2(70)
^{59}Zn	2 837.21(91)[d]	2 890(40)	−53(40)
^{60}Zn	5 104.93(51)	5 120(11)	−15(11)
^{60}Ga[b]	73(110)	26(120)	50(160)
^{61}Ga[b]	207(50)	192(50)	15(80)

[a]The value of the proton-decay daughter of the nuclide has been taken from Ref. [29].
[b]The mass excess value for the proton-decay daughter is from this work whereas the mass excess value for the nuclide is from Ref. [29].
[c]The mass excess value for the proton-decay daughter ^{54}Co was taken from Ref. [51].
[d]S_p calculated from the adjusted mass values given in Table III. The directly measured value, $S_p = 2836.9(12)$keV, is less precise owing to a large uncertainty in δr.

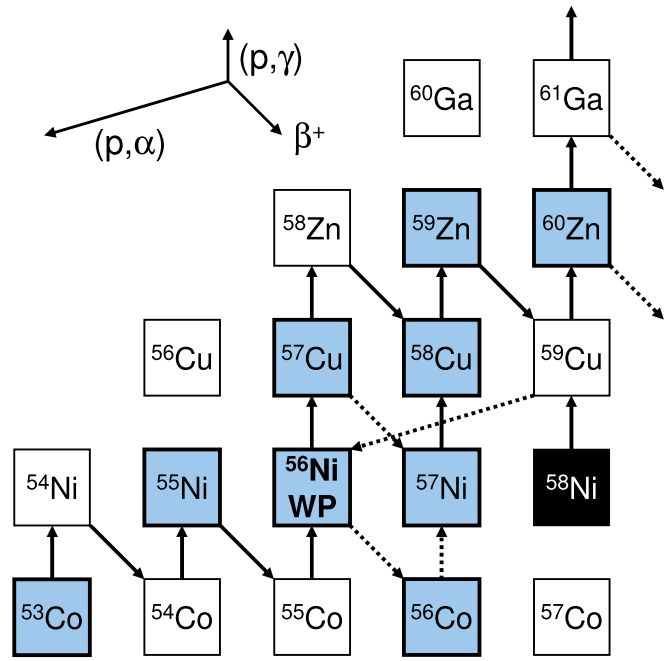

FIG. 12. (Color online) The rp-process path for steady-state burning conditions according to Ref. [4]. Shown are the reaction flows of more than 10% (solid line) and of 1%–10% (dashed line) of the reaction flow through the 3α reaction. All of the measured nuclides (highlighted) lie at the rp-process path flowing through the waiting-point (WP) nucleus ^{56}Ni.

for the nuclides shown in Fig. 12. This helps to do more reliable astrophysical calculations for the rp process. The rp-process path beyond the waiting-point nucleus ^{56}Ni is of special interest and is mainly determined by the ^{56}Ni$(p,\gamma)^{57}$Cu proton capture rate at lower temperatures (below ≈ 1 GK) and the β^+-decay rate of ^{58}Zn at higher temperatures. The reaction rate for ^{56}Ni$(p,\gamma)^{57}$Cu has been calculated in detail in Ref. [89].

The Q value for the reaction ^{56}Ni$(p,\gamma)^{57}$Cu has now been improved from 695(19) keV to 689.69(51) keV. A new reaction rate can be estimated with the new resonance energies $E_r = E_x - S_p$, where E_x is the excitation energy of the final state in ^{57}Cu and S_p is the proton separation energy for ^{57}Cu. The astrophysical reaction rate for resonant captures to states with resonance energies E_i and resonance strengths $\omega\gamma_i$ (both in MeV) is obtained by

$$N_A\langle\sigma v\rangle_r = 1.54\times10^{11}(\mu T_9)^{-3/2}\sum_i(\omega\gamma)_i \times \exp(-11.605E_i/T_9)\ \mathrm{cm^3mol^{-1}s^{-1}}. \quad (13)$$

The resonance strength $\omega\gamma$ for an isolated resonance in a (p,γ) reaction is given by

$$\omega\gamma = \frac{2J+1}{2(2J_t+1)}\frac{\Gamma_p\Gamma_\gamma}{\Gamma_{\mathrm{tot}}}, \quad (14)$$

where J and J_t are the spins of the resonance state and the target nucleus (^{56}Ni) and the total width Γ_{tot} is the sum of the proton width Γ_p and the γ width Γ_γ. The proton widths have

TABLE VII. Resonance parameters for the reaction ^{56}Ni$(p,\gamma)^{57}$Cu. The resonance energy E_r has been determined with the new JYFLTRAP S_p value for ^{57}Cu. The values of Γ_p have been scaled from Ref. [89] with new E_r values and the Γ_γ values are directly from [89].

E_x (keV)[a]	J_f[a]	E_r (MeV)	Γ_p (eV)[b]	Γ_γ (eV)[c]	$\omega\gamma$ (eV)
1 028(4)	$5/2^-$	0.338(4)	7.94×10^{-12}	3.55×10^{-4}	2.38×10^{-11}
1 106(4)	$1/2^-$	0.416(4)	2.26×10^{-7}	4.23×10^{-3}	2.26×10^{-7}
2 398(10)	$5/2^-$	1.708(10)	9.43×10^{-2}	1.37×10^{-2}	3.59×10^{-2}
2 520(25)	$7/2^-$	1.830(25)	7.29×10^{-2}	8.38×10^{-3}	3.01×10^{-2}

[a]From Ref. [91].
[b]Scaled from the values in Ref. [89]
[c]From Ref. [89].

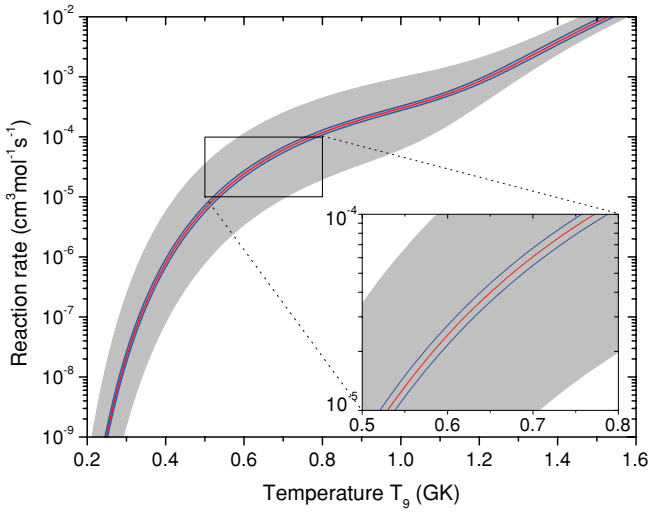

FIG. 13. (Color online) Total reaction rate for ^{56}Ni$(p,\gamma)^{57}$Cu. The gray-shaded area shows the calculated reaction rate with the old resonance energies including the uncertainties coming from the reduced mass μ, S_p for ^{57}Cu, and resonance energies E_i. The red curve has been plotted with the new JYFLTRAP values for the reduced mass and S_p of ^{57}Cu and the blue curves show the error band including the uncertainties in μ, S_p, and E_i. The inset shows the reaction rate between 0.5 and 0.8 GK. The precise S_p value reduces significantly the uncertainties of the calculated reaction rate.

now been scaled from Ref. [89] by using the relation

$$\Gamma_p \propto \exp\left(-31.29 Z_1 Z_2 \sqrt{\frac{\mu}{E_r}}\right), \tag{15}$$

where Z_1 and Z_2 are the proton numbers of the incoming particles, μ is the reduced mass in u, and E_r is the center-of-mass resonance energy in keV [90]. The resonance parameters are summarized in Table VII. The non-resonant reaction rate has been taken from [89] and scaled with the new value for the reduced mass.

The improved precision of the proton-capture Q value decreases the uncertainty of the calculated reaction rate dramatically as the rate depends exponentially on the Q value. With the new Q value, a factor of 4 in the uncertainty of the reaction rate at temperatures around 1 GK shown in Ref. [89] is removed, and the new rate is a little higher than calculated with the old Q value (see Fig. 13). The new Q value supports the conclusions of Ref. [89] that the lifetime of ^{56}Ni against proton capture is much shorter than in the previous works. This reduces the minimum temperature required for the rp process to proceed beyond ^{56}Ni. In fact, with the rates of Ref. [89], this temperature threshold coincides with the temperature for the breakout of the hot CNO cycles.

V. SUMMARY AND CONCLUSIONS

In conclusion, atomic masses in the vicinity of the doubly magic ^{56}Ni nucleus have been measured with the JYFLTRAP Penning trap mass spectrometer. Frequency ratios measured between 13 nuclides close to $A = 56$ formed an overdetermined network for which a least-squares minimization has been done. The adjusted mass values have improved the precisions of the AME03 mass values remarkably. The most surprising deviations from the AME03 values have been found at $A = 58$. The AME03 value for ^{58}Cu based on (p, n) threshold energy measurements deviates from the value obtained in this work by 2.2σ. For ^{58}Ni, a 1σ deviation from the AME03 value has been found, but the value agrees almost perfectly with the older (n, γ) results for ^{58}Ni [62,63]. In addition, the mass values obtained for ^{55}Co, ^{59}Zn, and ^{60}Zn deviate from the AME03 values by 1.3σ–1.4σ.

The excitation energy of the proton-emitting $19/2^-$ isomeric state in ^{53}Co has been improved and the decay scheme of ^{53}Co revised. The Q_{EC} values for $T = 1/2$ mirror transitions of ^{53}Co, ^{55}Ni, ^{57}Cu, and ^{59}Zn have been measured directly. These values are useful for precise weak-interaction information and a possible derivation of $|V_{ud}|$ in future, when either of the β or neutrino asymmetry parameters or $\beta-\nu$ angular correlation coefficient has been measured precisely enough. Coulomb displacement energies between isobaric analog states have been determined from these mirror Q_{EC} values and from the Q_{EC} values of ^{56}Ni and ^{58}Cu. The new Q_{EC} value for the ^{58}Cu ground state β decay allowed a revised B(GT) value for this transition used as a calibrant in ^{58}Ni(^{3}He, t) charge-exchange reaction studies. All measured nuclides lie at the path of the astrophysical rp process for which the improved S_p and Q_{EC} values are important. In particular, we have directly measured the Q value for the proton capture on ^{56}Ni, which removes the large uncertainties in the corresponding reaction rate at lower temperatures. The new result supports the conclusions of earlier works that the rp process can proceed beyond ^{56}Ni.

ACKNOWLEDGMENTS

This work has been supported by the EU Sixth Framework program "Integrating Infrastructure Initiative—Transnational Access," Contract No. 506065 (EURONS) and by the Academy of Finland under the Finnish Centre of Excellence Programme (Nuclear and Accelerator Based Physics Programme at JYFL). A.K. acknowledges the support from the Academy of Finland under the Project No. 127301.

[1] H. Schatz *et al.*, Phys. Rep. **294**, 167 (1998).
[2] M. T. F. da Cruz, Y. Chan, R.-M. Larimer, K. T. Lesko, E. B. Norman, R. G. Stokstad, F. E. Wietfeldt, and I. Žlimen, Phys. Rev. C **46**, 1132 (1992).
[3] R. K. Wallace and S. E. Woosley, Astrophys. J. Suppl. Ser. **45**, 389 (1981).
[4] H. Schatz, A. Aprahamian, V. Barnard, L. Bildsten, A. Cumming, M. Ouellette, T. Rauscher, F.-K. Thielemann, and M. Wiescher, Phys. Rev. Lett. **86**, 3471 (2001).
[5] V.-V. Elomaa *et al.*, Phys. Rev. Lett. **102**, 252501 (2009).
[6] J. Cerny, J. E. Esterl, R. A. Gough, and R. G. Sextro, Phys. Lett. B **33**, 284 (1970).

[7] J. Cerny, R. A. Gough, R. G. Sextro, and J. E. Esterl, Nucl. Phys. A **188**, 666 (1972).
[8] N. Severijns, M. Tandecki, T. Phalet, and I. S. Towner, Phys. Rev. C **78**, 055501 (2008).
[9] O. Naviliat-Cuncic and N. Severijns, Phys. Rev. Lett. **102**, 142302 (2009).
[10] J. Äystö, Nucl. Phys. A **693**, 477 (2001).
[11] V.-V. Elomaa *et al.*, Eur. Phys. J. A **40**, 1 (2009).
[12] G. Audi, O. Bersillon, J. Blachot, and A. H. Wapstra, Nucl. Phys. A **729**, 3 (2003).
[13] V.-V. Elomaa, T. Eronen, J. Hakala, A. Jokinen, A. Kankainen, I. D. Moore, S. Rahaman, J. Rissanen, C. Weber, and J. Äystö, Nucl. Instrum. Methods Phys. Res. Sect. A **612**, 97 (2009).
[14] J. Huikari, P. Dendooven, A. Jokinen, A. Nieminen, H. Penttilä, K. Peräjärvi, A. Popov, S. Rinta-Antila, and J. Äystö, Nucl. Instrum. Methods Phys. Res. Sect. B **222**, 632 (2004).
[15] A. Kankainen *et al.*, Eur. Phys. J. A **29**, 271 (2006).
[16] C. Weber *et al.*, Phys. Rev. C **78**, 054310 (2008).
[17] S. Rahaman *et al.*, Phys. Lett. B **662**, 111 (2008).
[18] A. Nieminen, J. Huikari, A. Jokinen, J. Äystö, P. Campbell, E. C. A. Cochrane, and (EXOTRAPS Collaboration), Nucl. Instrum. Methods Phys. Res. Sect. A **469**, 244 (2001).
[19] V. S. Kolhinen *et al.*, Nucl. Instrum. Methods Phys. Res. Sect. A **528**, 776 (2004).
[20] G. Savard, St. Becker, G. Bollen, H.-J. Kluge, R. B. Moore, Th. Otto, L. Schweikhard, H. Stolzenberg, and U. Wiess, Phys. Lett. A **158**, 247 (1991).
[21] G. Gräff, H. Kalinowsky, and J. Traut, Z. Phys. A **297**, 35 (1980).
[22] M. König, G. Bollen, H.-J. Kluge, T. Otto, and J. Szerypo, Int. J. Mass Spectrom. Ion Processes **142**, 95 (1995).
[23] G. Gabrielse, Phys. Rev. Lett. **102**, 172501 (2009).
[24] S. George, K. Blaum, F. Herfurth, A. Herlert, M. Kretzschmar, S. Nagy, S. Schwarz, L. Schweikhard, and C. Yazidjian, Int. J. Mass Spectrom. **264**, 110 (2007).
[25] M. Kretzschmar, Int. J. Mass Spectrom. **264**, 122 (2007).
[26] T. Eronen *et al.*, Phys. Rev. Lett. **103**, 252501 (2009).
[27] A. Kellerbauer, K. Blaum, G. Bollen, F. Herfurth, H.-J. Kluge, M. Kuckein, E. Sauvan, C. Scheidenberger, and L. Schweikhard, Eur. Phys. J. D **22**, 53 (2003).
[28] R. T. Birge, Phys. Rev. **40**, 207 (1932).
[29] G. Audi, A. H. Wapstra, and C. Thibault, Nucl. Phys. A **729**, 337 (2003).
[30] G. Audi, W. G. Davies, and G. E. Lee-Whiting, Nucl. Instrum. Methods Phys. Res. Sect. A **249**, 443 (1986).
[31] M. Mukherjee *et al.*, Eur. Phys. J. A **35**, 31 (2008).
[32] D. Mueller, E. Kashy, W. Benenson, and H. Nann, Phys. Rev. C **12**, 51 (1975).
[33] S. J. Williams *et al.*, Phys. Rev. C **68**, 011301(R) (2003).
[34] M. A. Bentley and S. M. Lenzi, Prog. Part. Nucl. Phys. **59**, 497 (2007).
[35] I. D. Proctor, W. Benenson, J. Dreisbach, E. Kashy, G. F. Trentelman, and B. M. Preedom, Phys. Rev. Lett. **29**, 434 (1972).
[36] D. Mueller, E. Kashy, and W. Benenson, Phys. Rev. C **15**, 1282 (1977).
[37] J. Äystö, J. Ärje, V. Koponen, P. Taskinen, H. Hyvönen, A. Hautojärvi, and K. Vierinen, Phys. Lett. B **138**, 369 (1984).
[38] C. G. Hoot, M. Kondo, and M. E. Rickey, Nucl. Phys. **71**, 449 (1965).
[39] R. G. Miller and R. W. Kavanagh, Nucl. Phys. A **94**, 261 (1967).
[40] E. K. Johansson *et al.*, Phys. Rev. C **77**, 064316 (2008).
[41] T. Shinozuka, M. Fujioka, H. Miyatake, M. Yoshii, H. Hama, and T. Kamiya, Phys. Rev. C **30**, 2111 (1984).
[42] B. Sherrill, K. Beard, W. Benenson, C. Bloch, B. A. Brown, E. Kashy, J. A. Nolen, Jr., A. D. Panagiotou, J. van der Plicht, and J. S. Winfield, Phys. Rev. C **31**, 875 (1985).
[43] C. A. Gagliardi, D. R. Semon, R. E. Tribble, and L. A. Van Ausdeln, Phys. Rev. C **34**, 1663 (1986).
[44] E. Stiliaris, H. G. Bohlen, X. S. Chen, B. Gebauer, A. Miczaika, W. von Oertzen, W. Weller, and T. Wilpert, Z. Phys. A **326**, 139 (1987).
[45] J. M. Freeman, J. H. Montague, G. Murray, R. E. White, and W. E. Burcham, Nucl. Phys. **65**, 113 (1965).
[46] B. E. Bonner, G. Rickards, D. L. Bernard, and G. C. Phillips, Nucl. Phys. **86**, 187 (1966).
[47] J. C. Overley, P. D. Parker, and D. A. Bromley, Nucl. Instrum. Methods Phys. Res. Sect. A **68**, 61 (1969).
[48] D. Rudolph *et al.*, Eur. Phys. J. A **14**, 137 (2002).
[49] J. M. Freeman, Nucl. Instrum. Methods **134**, 153 (1976).
[50] J. B. Marion, Rev. Mod. Phys. **38**, 660 (1966).
[51] T. Eronen *et al.*, Phys. Rev. Lett. **100**, 132502 (2008).
[52] Y. Arai, M. Fujioka, E. Tanaka, T. Shinozuka, H. Miyatake, M. Yoshii, and T. Ishimatsu, Phys. Lett. B **104**, 186 (1981).
[53] B. Sherrill, K. Beard, W. Benenson, B. A. Brown, E. Kashy, W. E. Ormand, H. Nann, J. J. Kehayias, A. D. Bacher, and T. E. Ward, Phys. Rev. C **28**, 1712 (1983).
[54] M. B. Greenfield, C. R. Bingham, E. Newman, and M. J. Saltmarsh, Phys. Rev. C **6**, 1756 (1972).
[55] H. Kawakami, S. Shibata, J. Tanaka, T. Toriyama, S. Noguchi, M. Mushano, and K. Hisatake, J. Phys. Soc. Jpn. **55**, 3014 (1986).
[56] D. J. Martin, J. R. Leslie, W. Mclatchie, C. F. Monahan, and L. E. Carlson, Nucl. Phys. A **187**, 337 (1972).
[57] B. Erlandsson and J. Lyttkens, Z. Phys. A **280**, 79 (1977).
[58] R. Hänninen and G. U. Din, Phys. Scr. **22**, 439 (1980).
[59] J. D. Goss, C. P. Browne, and A. A. Rollefson, Phys. Rev. Lett. **30**, 1255 (1973).
[60] P. L. Jolivette, J. D. Goss, G. L. Marolt, A. A. Rollefson, and C. P. Browne, Phys. Rev. C **10**, 2449 (1974).
[61] H. Pettersson, O. Bergman, and C. Bergman, Ark. Fys. **29**, 423 (1965).
[62] W. M. Wilson, G. E. Thomas, and H. E. Jackson, Phys. Rev. C **11**, 1477 (1975).
[63] A. F. M. Ishaq, A. Robertson, W. V. Prestwich, and T. J. Kennett, Z. Phys. A **281**, 365 (1977).
[64] Z. Guo, C. Alderliesten, C. van der Leun, and P. M. Endt, Nucl. Phys. A **540**, 117 (1992).
[65] P. Spilling, H. Gruppelaar, H. F. De Vries, and A. M. J. Spits, Nucl. Phys. A **113**, 395 (1968).
[66] D. E. Alburger, Nucl. Instrum. Methods Phys. Res. **136**, 323 (1976).
[67] M. L. Stelts and R. E. Chrien, Nucl. Instrum. Methods Phys. Res. **155**, 253 (1978).
[68] M. A. Islam, T. J. Kennett, S. A. Kerr, and W. V. Prestwich, Can. J. Phys. **58**, 168 (1980).
[69] R. Vennink, J. Kopecky, P. M. Endt, and P. W. M. Glaudemans, Nucl. Phys. A **344**, 421 (1980).
[70] H. Nann, E. Kashy, D. Mueller, A. Saha, and S. Raman, Phys. Rev. C **14**, 2338 (1976).
[71] C. Guénaut *et al.*, Phys. Rev. C **75**, 044303 (2007).
[72] A. Harder, S. Michaelsen, K. P. Lieb, and A. P. Williams, Z. Phys. A **345**, 143 (1993).
[73] S. Raman (private communication from Ref. [29]).

[74] R. B. Firestone *et al.*, IAEA report No. Tecdoc 5, 2003.
[75] R. O. Bondelid and J. W. Butler, Phys. Rev. **130**, 1078 (1963).
[76] I. Fodor, I. Szentpétery, and J. Szücs, Phys. Lett. B **32**, 689 (1970).
[77] H. V. Klapdor, M. Schrader, G. Bergdolt, and A. M. Bergdolt, Nucl. Phys. A **245**, 133 (1975).
[78] H. Junde, Nucl. Data Sheets **87**, 507 (1999).
[79] [http://www.nndc.bnl.gov/logft/].
[80] I. S. Towner and J. C. Hardy, Rep. Prog. Phys. **73**, 046301 (2010).
[81] Particle Data Group, Phys. Lett. B **667**, 31 (2008).
[82] H. Fujita *et al.*, Phys. Rev. C **75**, 034310 (2007).
[83] J. M. Freeman, J. H. Montague, G. Murray, R. E. White, and W. E. Burcham, Nucl. Phys. **69**, 433 (1965).
[84] K. Peräjärvi *et al.*, Nucl. Phys. A **696**, 233 (2001).
[85] Z. Janas *et al.*, Eur. Phys. J. A **12**, 143 (2001).
[86] H. W. Jongsma, A. G. Da Silva, J. Bron, and H. Verheul, Nucl. Phys. A **179**, 554 (1972).
[87] M. S. Antony, A. Pape, and J. Britz, At. Data Nucl. Data Tables **66**, 1 (1997).
[88] J. K. Tuli, Nucl. Data Sheets **100**, 347 (2003).
[89] O. Forstner, H. Herndl, H. Oberhummer, H. Schatz, and B. A. Brown, Phys. Rev. C **64**, 045801 (2001).
[90] C. E. Rolfs and W. S. Rodney, in *Cauldrons in the Cosmos*, edited by D. N. Schramm (University of Chicago Press, Chicago, 1988).
[91] M. R. Bhat, Nucl. Data Sheets **85**, 415 (1998).